PAPER

Nonlinear wave-particle interaction behaviors driven by energetic ions in the HL-2A Tokamak

IOP Publishing | International Atomic Energy Agency Nuclear Fusion

Nucl. Fusion **58** (2018) 096028 (8pp) https://doi.org/10.1088/1741-4326/aacf46

Nonlinear wave-particle interaction behaviors driven by energetic ions in the HL-2A Tokamak

Y.M. Hou[1,2], W. Chen[2], Y. Yu[1], M. Lesur[3], X.R. Duan[2], M. Xu[2], M.Y. Ye[1] and HL-2A Team[2]

[1] School of Physical Sciences, University of Science and Technology of China, Hefei, Anhui 230026, China
[2] Southwestern Institute of Physics, Post Office Box 432, Chengdu 610041, China
[3] Institut Jean Lamour, Universite de Lorraine, BP 50840, Nancy 54011, France

E-mail: houym@swip.ac.cn and chenw@swip.ac.cn

Received 1 March 2018, revised 24 June 2018
Accepted for publication 27 June 2018
Published 12 July 2018

Abstract

Frequency chirping properties of Alfvén modes driven by energetic ions in HL-2A have been analyzed with a method based on the so-called Berk–Breizman model, which predicts that the interaction between wave, energetic ions and collision effects may exhibit steady-state, periodic, chaotic and explosive regimes. Nonlinear wave-particle interaction behaviors with chirping structures observed in HL-2A belongs to the chaotic regime. Those four typical unstable regimes are reproduced by a simulation code with two collision models: pure diffusion and pure Krook operator. As known, frequency shifts nonlinearly, from the linear eigenfrequency, as phase space holes and clumps move upward and downward respectively from original resonance region. In this paper, typical unstable chirping events observed in HL-2A are presented, and bulk plasma parameters are provided for the identification of TAEs, RSAEs and BAEs. Alfvén instabilities including TAEs with up-down and main-downward hooked chirping, RSAEs with up-sweeping and down-sweeping chirping, BAEs with up-down and main-downward chirping in HL-2A are discussed in this work. Comparing up-down and main-downward chirping plasma parameters of TAEs and BAEs, we assume that lower density, higher electron temperature would mean higher beam beta, stronger drive, and stronger collision operators. Furthermore, two codes based on BB model, δf-COBBLES and BOT, are applied to up-down TAEs, and both Krook and Fokker–Plank collision models are considered. Comparing the amplitude of perturbations between experimental observation and calculation, the δf-COBBLES with Fokker–Plank collision model yields better qualitative and quantitative agreement. Though the spectrum obtained by BOT code does not show good agreements with lifetime and frequency, it shows a qualitative agreement. As for TAEs with main-downward frequency chirping, only BOT with Fokker–Plank model could show a qualitative agreement. Comparing the collision operators of up-down and main-downward chirping, main-downward chirping correlated with stronger collision operators.

Keywords: energetic ions, Alfvén modes, frequency chirping properties

(Some figures may appear in colour only in the online journal)

1. Introduction

MHD waves driven by energetic ions in toroidal magnetic confinement devices attract increasing attention. They are considered as desirable channels for energy [1] and momentum [2] transfer from resonant fast ions to thermal ions in ITER. Besides, they can also provide valuable information about the key plasma parameters, which is important for future burning plasma. However, the consequences of wave-particle interactions may be undesirable. They may redistribute and eject a large fraction of energetic ions from plasmas [3, 4], subsequently damage on the first wall and degrade plasma confinement. They may also impact background plasma turbulence and transport barriers [5, 6]. Thus nonlinear interaction between MHD waves and energetic ions is an essential element for the research of fusion reactors [7–10].

A universal feature of energetic particle-driven modes, is their nonlinear, fast frequency sweeping, called as chirping, observed in numerous fusion plasmas. What's more, frequency chirping of Alfvén modes are common nonlinear wave-particle interaction behaviors in many magnetic confinement devices. Experimental observations have proved that NBI and ICRH may excite TAEs with chirping characters, NBI driven instabilities were observed in DIII-D [11], JT-60U [12], MAST [13], NSTX [14], HL-2A [15], and ICRH driven instabilities were observed in JT-60U [16], JET [17], DIII-D [18], C-MOD [19].

A general theory (called BB model) which extends the bump-on-tail model was first proposed to elucidate the production of frequency chirping [20, 21]. It shows that the chirping arises from the spontaneous excitation of phase-space structures in resonance region, with the evolution of hole and clump pairs in the energetic ion distribution. Numerical studies based on the BB model have been applied to the TAEs instabilities, such as BOT used for MAST [22], δf-COBBLES used for JT-60U [23, 24]. In addition, BAEs with chirping characters have also been investigated by the Berk–Breizman model [25, 26].

As an extension of the Vlasov–Poisson system, the BB model describes the time evolution a bump-on-tail velocity distribution, with a Maxwellian bulk, a weak beam, and a small electrostatic perturbation. This simplified model enables more understanding of nonlinear wave-particle interaction in complex plasma geometries. The background dissipative mechanisms are assumed as external wave damping and a collision operator. Then the nonlinear perturbation could be damped or amplified by adjusting the parameters of the kinetic system model. When perturbation acts on the resonance region of the distribution function, a local plateau is caused via the phase mixing of those resonant particles. Further, the balance between the sink and the source of energetic ions result to the mode saturation. To investigate the rich physics in wave-particle interactions, a particle annihilation model Krook operator within the annihilation rate v_α.

They obtained a representative equation for the normalized wave amplitude A [20],

$$\frac{\mathrm{d}A}{\mathrm{d}\tau} = A(\tau) - \frac{1}{2}\int_0^{\tau/2} \mathrm{d}z z^2 A(\tau - z) \times \int_0^{\tau-2z} \mathrm{d}x \, \exp[-\hat{v}_\alpha(2z+x)] \times A(\tau - z - x)A(\tau - 2z - x). \quad (1)$$

Where $\tau = (\gamma_L - \gamma_d)t, \hat{v}_\alpha = v_\alpha/(\gamma_L - \gamma_d)$, γ_L is the kinetic drive in the absence of dissipation, γ_d is the intrinsic damping rate from the background plasmas. Since the growth rate of chirping structure is neither γ or γ_L and the decay rate is not simply γ_d but a function of several linear parameters. Numerical solutions of equation (1) show that four typical regimes of marginally unstable amplitude evolutions are exhibited, namely steady-state, periodic, chaotic and explosive. Later, many authors confirmed that the chaotic regime significantly account for mode chirping in experiments.

Based on BB model, more theoretical progress has been done to interpret the frequency chirping event. An extension of equation (1) was introduced by Lilley [22].

$$\frac{\mathrm{d}A}{\mathrm{d}\tau} = A(\tau) - \frac{1}{2}\int_0^{\tau/2} \mathrm{d}z z^2 A(\tau - z) \times \int_0^{\tau-2z} \mathrm{d}x \exp[-\hat{v}_d^3 z^2\left(\frac{2z}{3} + x\right) - \hat{v}_\alpha(2z+x) + \mathrm{i}\hat{v}_f^2 z(z+x)] \times A(\tau - z - x)A^*(\tau - 2z - x). \quad (2)$$

Where $\hat{v}_d^3 = v_d^3/(\gamma_L - \gamma_d)^3$, $\hat{v}_f^2 = v_f^2/(\gamma_L - \gamma_d)^2$, v_d, v_f and v_α respectively represent velocity-space diffusion, dynamical friction (drag) and Krook collision. While v_d includes contribution from the pitch-angle scattering term and parallel velocity diffusion, v_f includes contribution from the slowing down term, pitch-angle scattering term and parallel velocity diffusion. To investigate the effect of dynamical friction on the marginal stability kinetic system, with the help of BOT code based on BB model, nonlinear behaviors, such as hooked frequency chirping, undulating, and steady state regimes were obtained in the presence of both drag and diffusion. According to the results, dynamical friction has a destabilizing effect on perturbed distribution function [27–29].

According to the TAEs chirping characteristics, such as sweeping-rate, lifetime, and frequency, analytic and semi-empirical laws were developed and applied to JT-60U [24]. A kinetic code COBBLES based on BB theory was developed, with two versions, perturbative (δf) and self-consistent (full-f). With this code, both Krook and Fokker–Plank collision operators were applied to TAEs, but the Fokker–Plank collision model yielded better qualitative and quantitative agreement. Besides, it was verified that TAEs may exist far from marginal stability. Furthermore, hooked up-chirping events were also obtained with the COBBLES code [30].

The remain of this paper is organized as follows: section 2 describes the experimental conditions and observation of Alfvén instabilities including TAEs with up-down and main-downward hooked chirping, RSAEs with up- and down-sweeping chirping, and BAEs with up-down and main downward chirping in HL-2A tokamak. Section 3 deals with the analysis of nonlinear behaviors based on the BB model and numerical codes. Four typical unstable regimes are reproduced. Up-down and main-downward chirping TAEs are reproduced by δf-COBBLES and BOT. Section 4 presents the conclusion.

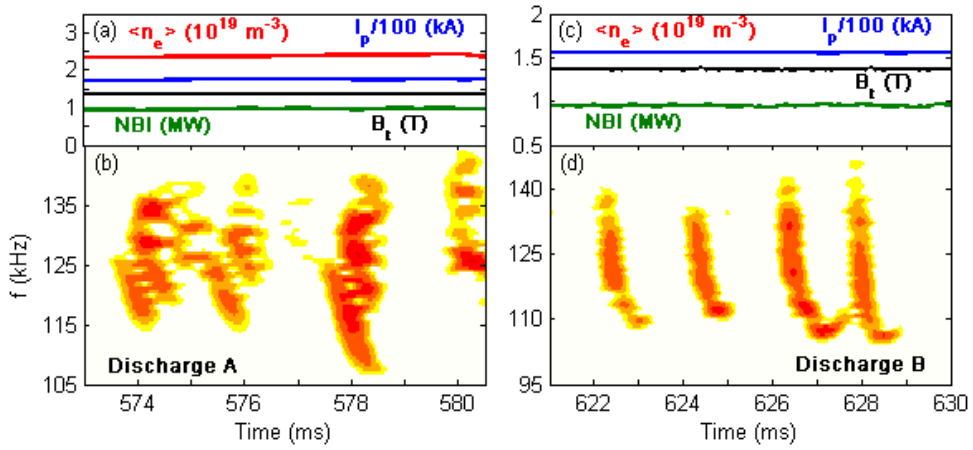

Figure 1. (*a*) The parameters of the discharge A, with line-averaged density $\langle n_e \rangle = 2.4 \times 10^{19}$ m^{-3}, current $I_p = 170$ kA, magnetic field $B_t = 1.35$ T, power of NBI $P_{NBI} = 1$ MW. (*b*) Example of TAEs with up-down chirping. (*c*) The plasma parameters of the discharge B, $\langle n_e \rangle = 1.5 \times 10^{19}$ m^{-3}, $I_p = 157$ kA, $B_t = 1.35$ T, $P_{NBI} = 1$ MW. (*d*) Example of TAEs with main-downward chirping.

2. Experimental observation

Studies of Alfvén instabilities in HL-2A have been carried out in previous works [31–34]. In terms of experimental conditions, the HL-2A has a low aspect ratio with minor radius $a = 40$ cm, major radius $R = 165$ cm. It operates in deuterium plasma with toroidal plasma current $I_p \sim 160$ kA, toroidal magnetic field $B_t \sim 1.3$ T, and electron density $n_e = 1.0 \sim 5.0 \times 10^{19}$ m^{-3}. Moreover, there are two main auxiliary heating systems, co-injection neutral-beam injection (NBI) with $P_{NBI}/E_b \sim 1.0$ MW/45 keV), and electron cyclotron resonance heating (ECRH), with $f/P_{ECRH} \sim 68$ GHz/3 MW. Diagnostic systems in HL-2A include the line-averaged density and the electron temperature, which are obtained by the hydrogen cyanide interferometer (HCN) and the multi-channel electron cyclotron emission (ECE), respectively. Besides, analysis of the Mirnov-coil data reveals the mode numbers and spectrograms of Alfvén modes.

Instabilities related to TAEs modes were observed and analyzed in HL-2A. In figure 1, we can distinguish two types of typical frequency chirping modes, up-down (discharge A) and main-downward chirping (discharge B). The figure 1(*a*) includes the essential parameters of the discharge A as a function of time. As for electron temperature measurements, TLS has poor time resolution, ECE has terrible performance when density is high in HL-2A. As for ion temperature measurements, CXRS is not always accessible. Thus electron and ion temperature are not always available. Figure 1(*b*) shows spectral analysis of magnetic fluctuations from Mirnov-coil, with the linear mode frequency $f \approx 126$ kHz, frequency shift $\delta f \approx 11.5$ kHz, frequency chirping lifetime $\tau_{ch} \approx 0.5$ ms, and chirping period $\Delta t_{ch} \approx 2$ ms.

As the magnetic field and the plasma current profile are flat during the chirping timescale, the frequency of the TAE mode is theoretically obtained: $\omega_{TAE} = V_A/2qR$, where $V_A = B_0/\sqrt{\mu_0 \rho}$ is the Alfvén velocity, $q = (m + 1/2)/n$, m is the poloidal mode number, n is the toroidal mode number. It is identified as an $m/n = 3/3$ and 4/3 TAE mode, so the theoretical frequency of TAEs in discharge A is $f = \omega_{TAE}/2\pi \approx 130$ kHz. In terms of measured frequency, it chirps between 114 and 137 kHz around the theoretical TAE frequency.

The properties of TAEs with main-downward frequency chirping are investigated in [15], but the excitation mechanism is still unknown. In [35], results of simulation show the ratio of specific heats will alter the chirping direction. In this paper, the BB model is not ready for explaining the role of specific heat, kinetic effects such as kinetic particle compression and radial non-uniformity, but focus on the collision operators. Though the hooked frequency spectrum was also analyzed theoretically in [24, 27], it was dominant upward frequency chirping that largely depend on the drag destabilizing effect. Figure 1(*d*) shows the frequency spectrum of TAEs with main-downward hooked chirping in HL-2A, with $m/n = 5/3$, ≈ 142 kHz, $\delta f \approx 32$ kHz, $\tau_{ch} \approx 1$ ms, $\Delta t_{ch} \approx 2$ ms.

The excitation of up- (discharge C) and down-sweeping (discharge D) reversed shear Alfvén Eigenmodes (RSAEs) in HL-2A have been explored in previous works [33]. Experimentally, as shown in figure 2(*b*), the frequency sweeps up from 68 to 92 kHz before the sawtooth collapse. As the frequency of RSAEs are related to the value of $q_{min}(t)$, which is changeable over time, the RSAEs frequency changes at a rate:

$$\frac{\mathrm{d}}{\mathrm{d}t}\omega_{RSAE}(t) \approx \pm m \frac{v_A}{R} \frac{\mathrm{d}}{\mathrm{d}t} q_{min}(t). \tag{3}$$

The plus and minus signs in equation (3) imply the downward and upward frequencies of RSAEs. In this sense, the frequency of RSAEs can be obtained by the formula below:

$$\omega_{RSAE}^2 = \frac{V_A^2}{R^2}\left(n - \frac{m}{q_{min}}\right)^2 + \omega_{BAE}^2 + \gamma\omega^2 \tag{4}$$

$$\omega_{BAE}^2 \equiv \frac{2}{m_i R^2}\left(T_e + \frac{7}{4}T_i\right) \tag{5}$$

where m_i represents the ion mass, T_e and T_i respectively correspond to electric and ion temperature. The $\delta\omega$ includes corrections for fast ion pressure and finite pressure gradients and can be neglected in this discharge.

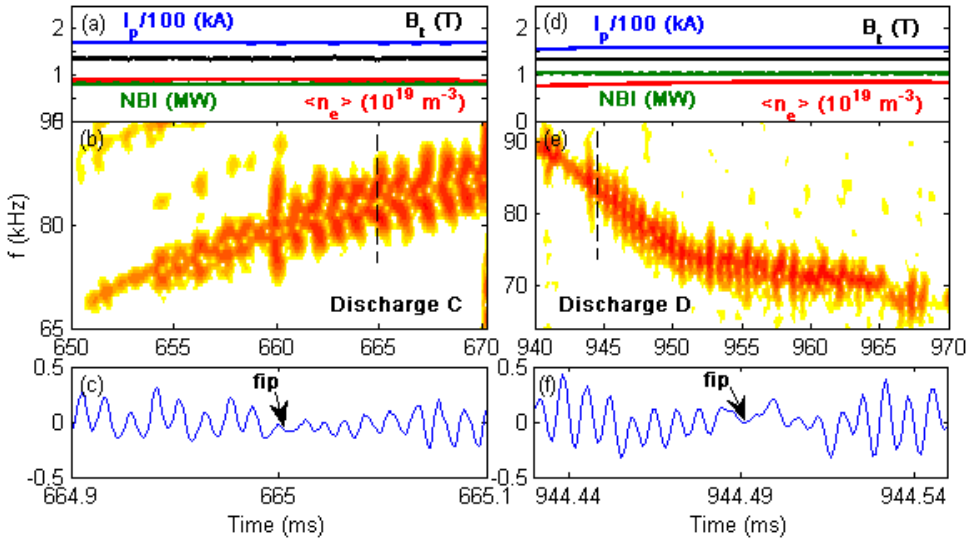

Figure 2. (*a*) The plasma parameters of the discharge C, $\langle n_e \rangle = 0.88 \times 10^{19}$ m^{-3}, $I_p = 169$ kA, $B_t = 1.33$ T, $P_{NBI} = 0.8$ MW. (*b*) Example of chirping RSAEs with upward sweeping. (*c*) and (*f*) Amplitude of the instability contains phase flips at every burst. (*d*) The plasma parameters of the discharge D, $\langle n_e \rangle = 0.86 \times 10^{19}$ m^{-3}, $I_p = 157$ kA, $B_t = 1.33$ T, $P_{NBI} = 1$ MW. (*e*) Example of chirping RSAEs with downward sweeping.

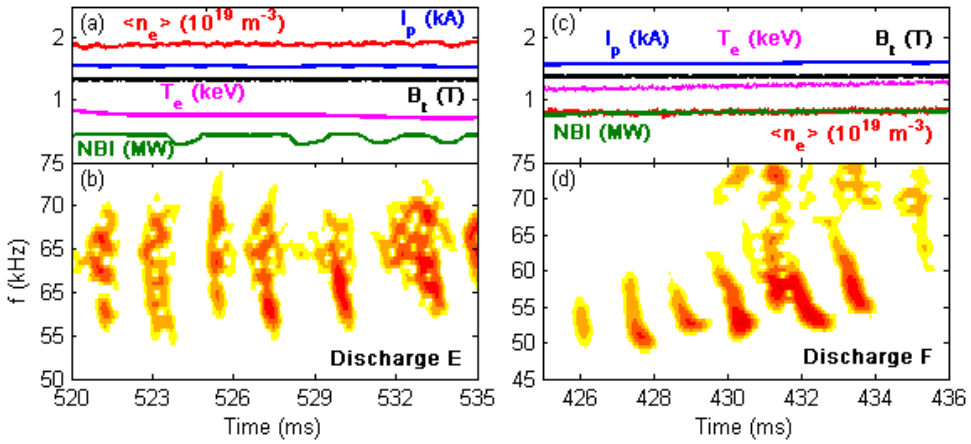

Figure 3. (*a*) The parameters of the discharge E: $\langle n_e \rangle = 1.9 \times 10^{19}$ m^{-3}, $I_p = 153$ kA, $B_t = 1.33$ T, $P_{NBI} = 0.45$ MW, $T_e = 0.77$ keV. (*b*) Example of BAEs with up-down chirping. (*c*) The parameters of the discharge F: $\langle n_e \rangle = 0.7 \times 10^{19}$ m^{-3}, $I_p = 158$ kA, $B_t = 1.37$ T, $P_{NBI} = 0.7$ MW, $T_e = 1.2$ keV. (*d*) Example of BAEs with main-downward chirping.

During the upward sweeping, it chirps up and down with $m/n = 2/2$, $\delta f \approx 6$ kHz, $\tau_{ch} \approx 0.5$ ms, $\Delta t_{ch} \approx 1$ ms, when $t = 665$ ms, $T_e = 1.7$ keV, $T_i = 1.5$ keV, $q_{min} \approx 1$, so the theoretical frequency of RSAEs in discharge C is $f \approx \omega_{BAE}/2\pi \approx 63.3$ kH. However, when $t = 665$ ms, $f \approx 78$–89 kHz, error bars in the experimental data may account for this discrepancy.

Oppositely, the down-sweeping RSAEs (see figure 2(*e*)) exists for tens of milliseconds, and it sweeps down from 90 kHz to 65 kHz. As the chirping velocity is much higher and the frequency chirping life time is much shorter, it seems like a straight line rather than a pitch fork. What's more, both of the amplitude of the instability (see figures 2(*c*) and (*f*)) contain phase flips at every burst.

Finally, β-induced Alfvén eigenmodes (BAEs) excited by electron or magnetic islands were investigated in previous works [31, 32]. BAEs with frequency chirping driven by energetic ions are observed in HL-2A. Two types of common BAEs with frequency chirping are shown in figure 3, up-down (discharge E) and main-downward chirping (discharge F). Figure 3(*b*) shows frequency chirps up from 63 to 70 kHz and down from 63 to 55 kHz in 0.5 ms, while chirping period $\Delta t_{ch} \approx 2$ ms. In terms of figure 3(*d*), the main-downward BAEs chirps down from ≈ 60 kHz, $\delta f \approx 10$ kHz, $\tau_{ch} \approx 0.8$ ms, $\Delta t_{ch} \approx 1.5$ ms.

Comparing to discharge A and C, discharge B and F have lower density corresponding to main-downward chirping. So we assume that lower density, higher T_e would mean higher beam beta, stronger drive, and stronger collision operators. For RSAEs, the q_{min} change leads to the frequency sweeping and is a linear phenomenon, though we assume the chirping character is correlated with pitch-fork structure, we could not analyze with COBBLES or BOT now. Further work should be extended and a better method may be applied.

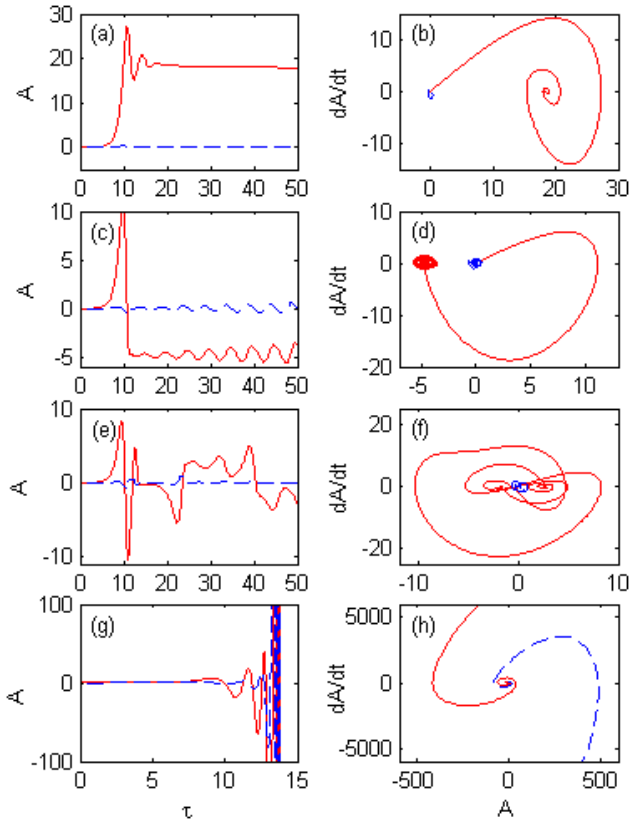

Figure 4. The translation from steady state to explosive regime for various values of v_d, while $v_\alpha = 0$, $v_f = 0$, $\varphi = \pi/1000$, $\gamma_L/\gamma = 1$, $\Delta t = 0.01$, $A_0 = 0.001$, (I) steady state saturation (*a*) and (*b*), $v_d = 4.2$; (II) periodic (*c*) and (*d*), $v_d = 2.13$; (III) chaotic (*e*) and (*f*), $v_d = 1.59$; (IV) explosive (*g*) and (*h*), $v_d = 1.1$. Left: time-evolution of wave amplitude A. Right: the change rate of A. The red line represents the real part and the blue dashed line represents the imaginary part.

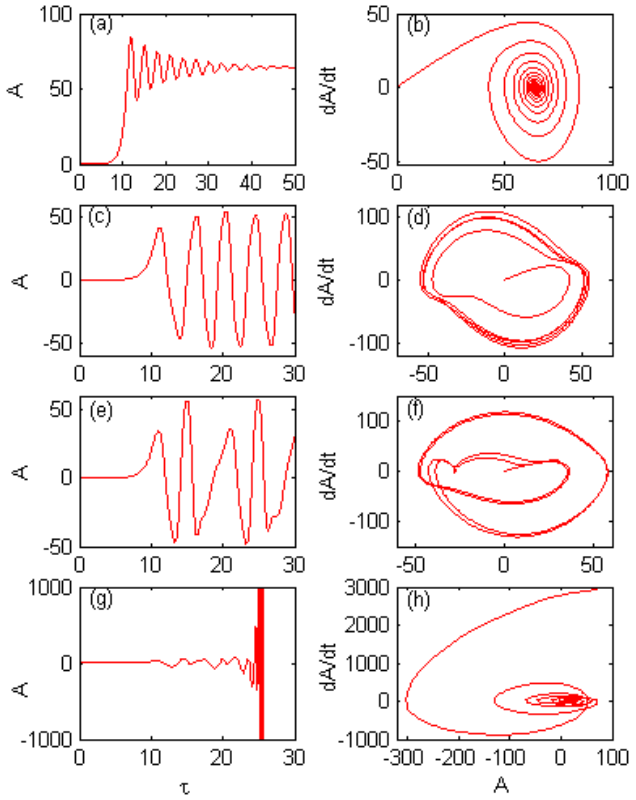

Figure 5. The translation from steady state saturation to explosive regime for various values of v_α, while $v_d = 0$, $v_f = 0$, $\varphi = 0$, $\gamma_L/\gamma = 0.5$, $\Delta t = 0.01$, $A_0 = 0.001$, (I) steady state saturation (*a*) and (*b*), $v_\alpha = 4.8$; (II) periodic (*c*) and (*d*), $v_\alpha = 2.9$; (III) chaotic (*e*) and (*f*), $v_\alpha = 2.5$; (IV) explosive (*g*) and (*h*), $v_\alpha = 2.3$. Left: time-evolution of wave amplitude A. Right: the change rate of A.

3. Analysis results

As mentioned in the section 1, the interaction between the wave and collisions affects wave amplitude and leads to four typical unstable regimes. Numerical solutions of equation (2) for various values of v_d shown in figure 4 (pure diffusion) and v_α shown in figure 5 (pure Krook operator) illustrate four examples of nonlinear saturation, corresponding to (I) steady state; (II) periodic; (III) chaotic; (IV) explosive.

In figure 4(*a*), for $v_d = 4.2$, the value of A reaches the stable value v_d^2 in a short time, in this steady state saturation, the change rate almost (see figure 4(*b*)) keeps at zero. In figure 4(*c*), for $v_d = 2.13$, the sign of A changes and the value undulates periodically around the stable value. In the periodic regime, the rate of change disturbs regularly in a sufficiently small range. In figure 4(*e*), as $v_d = 1.92$ the system goes into the unstable range, the oscillation value of A significantly exceeds the steady level and becomes irregular. Then bifurcations take place and destroy destroy the periodic limit cycle, corresponding to chaotic regime. However, the change rate indicates that mode amplitude is still limited in this regime. In figure 2(*g*), for $v_d = 1.1$ becomes much smaller, the effect of wave is predominant, and the system develops into an explosive regime that takes the solution out of the applicability range.

In figure 5(*a*), for $v_\alpha = 4.8$, the oscillation amplitude decreases gradually into a small value around $2\sqrt{2}v_\alpha^2$, the tracks of the change rate display as concentric circles. In figure 5(*c*), for $v_\alpha = 2.9$, the value of A oscillates periodically with the same amplitude, then the track of the change rate looks like a regular limit cycle. In figure 5(*e*), for $v_\alpha = 2.5$, the value of A vibrates with irregular period and amplitude, corresponding to an irregular closed limit cycle in the change rate track. In figure 5(*g*), for $v_\alpha = 2.3$, the mode breaks the steady level, and evolves into an explosive regime with considerable large amplitude and small period, hence the track of the change rate becomes unbounded.

Theoretical analysis and experimental studies for TAEs with frequency chirping have developed in the past decades [35–39]. We analyze the HL-2A experiments based on the BB model. Both δf-COBBLES and BOT are used to reproduce up-down chirping events. In the discharge A or B, the profile of background parameters is flat (see figure 1(*c*)), hence a fixed mode structure is assumed to reduce the problem to a 1D Hamiltonian.

As the frequency shifting is within the gap of the Alfvén continuum, we assume that chirping lifetime is determined by collision processes, but not by continuum damping. As

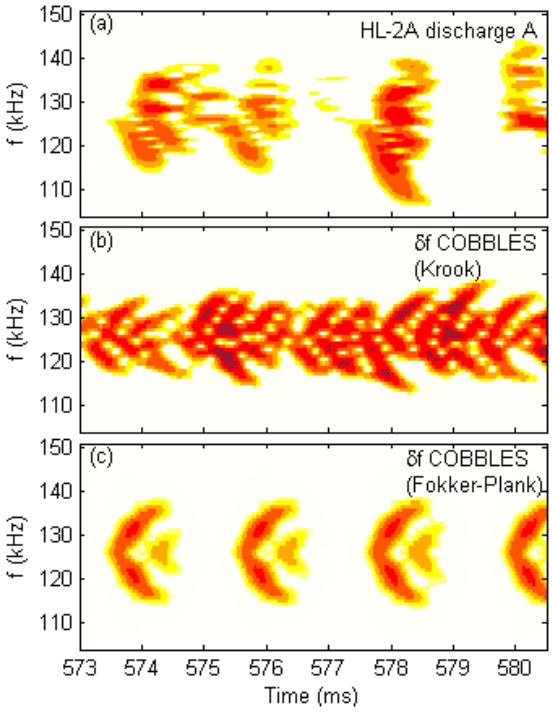

Figure 6. (*a*) The magnetic fluctuations spectrogram of discharge A featuring up-down chirping event. The δf-COBBLES simulation result spectrum obtained by Krook model (*b*) and Fokker–Plank model (*c*).

Table 1. The input parameters of δf-COBBLES estimated from the magnetic spectrogram of the discharge A, in percentage of the mode frequency ω.

Collison model	γ_{L0} (%)	γ_L (%)	γ_d (%)	ν_a (%)	ν_d (%)	ν_f (%)	γ (%)
Krook	6	5.5	4.7	0.28	…	…	0.78
Fokker–Planck	8	7.4	2	…	1.4	0.15	5.6

we intended to test two collision models: Krook and Fokker–Plank, empirical formulas for δf-COBBLES are employed for parameter setting [24]:

$$\gamma_{L0} \approx 1.3\left(\frac{1}{\varepsilon^2\mu^2}\frac{\mathrm{d}\delta\omega^2}{\mathrm{d}t}\right)^{1/3} \tag{6}$$

$$\gamma_d \approx 0.7\left(\frac{1}{\varepsilon^2\mu^2}\frac{\mathrm{d}\delta\omega^2}{\mathrm{d}t}\right)^{1/3}. \tag{7}$$

Where γ_{L0} is a measure of the slope of the initial velocity distribution, while γ_{L0} is given within roughly 30% error, and γ_d within 50% error. $\varepsilon \approx 0.44$, μ is the correction parameter, and $\mathrm{d}\delta\omega^2/\mathrm{d}t$ is the average chirping velocity obtained from experimental data.

In the Krook case:

$$\nu_\alpha \approx \frac{\iota_\alpha}{\tau_{\max}}. \tag{8}$$

Where $\iota_\alpha = 10$, $\tau_{\max}$ is frequency chirping lifetime obtained from experimental data.

In the Fokker–Plank case:

$$\nu_d \approx 1.2\left(\frac{\iota_\alpha}{\tau_{\max}}\right)^{2/3}\left(\frac{1}{\varepsilon^2\mu^2}\frac{\mathrm{d}\delta\omega^2}{\mathrm{d}t}\right)^{2/9}. \tag{9}$$

A fitting procedure of ν_d and ν_f was developed in [24].

We first focus on discharge A, magnetic spectrogram obtained by Mirnov-coils is shown in figure 6(*a*), numerical solution results obtained by code δf-COBBLES are shown in figures 6(*b*) and (*c*). Table 1 presents the parameters estimated from the magnetic spectrogram of the discharge, in percentage of the mode frequency $\omega = 2\pi f$.

From the results of trail and error fitting with the Krook model, we assume correction parameter $\mu = 0.8$, collision coefficient $\nu_\alpha = 0.28\%$. In figure 6(*b*), the simulation result spectrogram with δf-COBBLES Krook model displays discrepancies in frequency chirping period and shape. In the fitting procedure, the value of ν_α depends on frequency chirping time measured in experiment (see equation (8)), hence chirping velocity is decided by γ_L and γ_d.

Nevertheless, in figure 6(*c*) the simulation result spectrogram obtained by δf-COBBLES Fokker–Plank model shows qualitative and quantitative agreement with TAEs chirping structures measured in experiment. In this method, we assume $\mu = 0.95$, and $\nu_d = 1.4\%$, $\nu_f = 0.15\%$. As for ν_d and ν_f, when the effect of diffusion and drag increase, the chirping period decrease. As a caveat in this fitting procedure, the value of drag is underestimated [24]. With the increase of ν_f, the symmetry of chirping shape breaks and up-chirping structures are enhanced. What's more, energetic ion distribution function can also significantly affect the chirping asymmetry.

Once we accept the δf-COBBLES solution of discharge A (see table 1), then we could apply to BOT code. There are some differences in parameter setting. In terms of BOT code, ν_α, ν_d, ν_f are in units of $\gamma_L - \gamma_d$, while time is in units of γ_L, thus we could not obtain accuracy lifetime or frequency, more details about BOT code are shown in [27]. Table 2 presents the input parameters estimated from the table 1.

Figure 7 shows the BOT simulation results of discharge A with (*a*) Krook model and (*b*) Fokker–Plank model, respectively. Comparing with δf-COBBLES results (see figure 8), though the BOT code could not show good agreements in lifetime or frequency, it still performs well in qualitative analysis.

As for discharge B, the results of trail and error fitting with δf-COBBLES and BOT indicate BOT is more appropriate to reproduce main-downward chirping. Hence numerical solution results obtained by code BOT are shown in figures 8(*b*) and (*c*), with input parameters shown in table 3.

Magnetic spectrogram of discharge B obtained by Mirnov-coils is shown in figure 8(*a*). While we could not detail main-downward chirping from figure 8(*b*) obtained with the Krook model, which shows that Krook model is only applied to up-down chirping event analysis. In terms of Fokker–Plank model, comparing to table 2, $\gamma_d/\gamma_L \approx 0.9 > 0.27$, in this marginal critical regime ($\gamma_L - \gamma_d \ll \gamma_L$), the interplay of diffusion and drag effect results in system critical instability and strengthen the clump movement, leading to clump–clump interactions in the fast ion distribution function. As the value of ν_d and ν_f are much higher, we confirm that main-downward

Table 2. The input parameters of BOT code estimated from the table 1, v_α, v_d, v_f are in units of $\gamma_L - \gamma_d$. While time is in units of γ_L.

Collison model	γ_d / γ_L	$v_\alpha/(\gamma_L - \gamma_d)$	$v_d/(\gamma_L - \gamma_d)$	$v_f/(\gamma_L - \gamma_d)$
Krook	0.82	0.35	…	…
Fokker–Planck	0.27	…	0.26	0.028

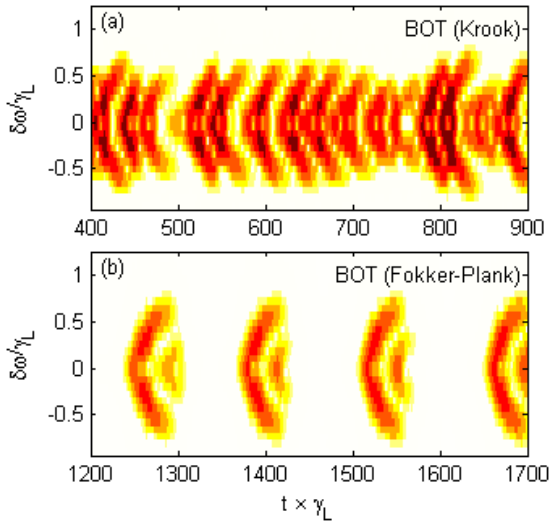

Figure 7. The BOT simulation results of discharge A with (*a*) Krook model and (*b*) Fokker–Plank model.

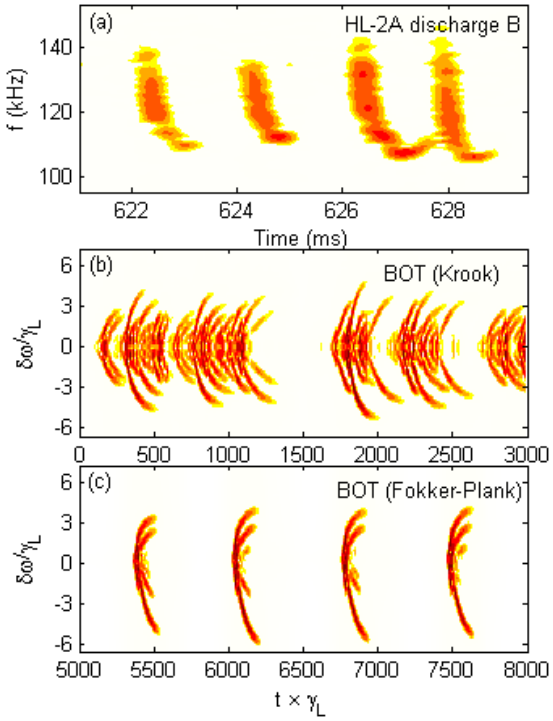

Figure 8. (*a*) The magnetic fluctuations spectrogram of discharge B featuring main-downward chirping event. A BOT simulation result spectrum with Krook (*b*) and Fokker–Plank model (*c*).

chirping regimes need stronger collision operators. The main-downward chirping means that clump movement, which indicates energy transfer from wave to particle, is dominant. In many magnetic confinement devices, Alfvén modes were observed with stronger drive, which means main-downward chirping may excited easier. It explains why main-downward chirping were observed more frequently.

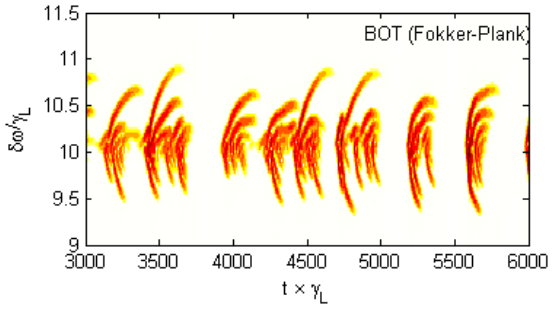

Figure 9. Example of a main-upward chirping event obtained by BOT with Fokker–Plank model.

Table 3. The input parameters of BOT applied to the discharge B. v_α, v_d, v_f are in units of $\gamma_L - \gamma_d$. While time is in units of γ_L.

Collison model	γ_d / γ_L	$v_\alpha/(\gamma_L - \gamma_d)$	$v_d/(\gamma_L - \gamma_d)$	$v_f/(\gamma_L - \gamma_d)$
Krook	0.9	0.09	…	…
Fokker–Planck	0.9	…	1.25	0.7725

Table 4. The input parameters of BOT contrary to the discharge B, v_α, v_d, v_f are in units of $\gamma_L - \gamma_d$. While time is in units of γ_L.

Collison model	γ_d / γ_L	$v_\alpha/(\gamma_L - \gamma_d)$	$v_d/(\gamma_L - \gamma_d)$	$v_f/(\gamma_L - \gamma_d)$
Fokker–Planck	0.9	…	1.25	1

Though the features of the main-downward chirping events (see figure 8(*c*)) qualitatively agree with the experimental spectrogram, discrepancies are apparent: abundant minor short-lived chirping events following every main chirping, which are absent in figure 8(*a*). Besides, in simulations, the up-chirping can be weaker by modulating input parameters, but cannot disappear absolutely, thus the codes that we applied to experiments are confined to symmetric and near-symmetric structures.

Figure 9 gives a contrary example of figure 8(*c*). The input parameters are shown in table 4. It's a main-upward chirping event. The increasing drag effect (v_f) strengthen the hole movements in fast ion distribution function, leading to intense hole–hole interaction [27, 30].

4. Summary

In this paper, example of up-down chirping and main-downward chirping TAEs and BAEs, up-sweeping and down-sweeping chirping RSAEs are observed. As discharge B and F with main-downward chirping events have lower density, we assume that lower density, higher T_e would mean higher beam beta, stronger drive, and stronger collision operators (v_α, v_d, v_f).

Then according to BB model, four typical unstable regimes are reproduced with two collision models. Figures 4 and 5 can help to understand the physics in the BB model, and 'dA/dt versus A' figures give some limit-cycle oscillation information which experimentalists care.

Both δf-COBBLES and BOT code based on BB model are applied to up-down chirping TAEs, Krook and Fokker–Plank model are considered. The δf-COBBLES with Fokker–Plank collision model yields better qualitative and quantitative agreement with discharge A consistently with [24]. The agreement concerns: growth and decay of perturbation amplitude, lifetime and chirping period. Though the BOT code could not show good agreements in lifetime or frequency, it still performs well in qualitative analysis.

Spectrum of TAEs with main-downward frequency chirping reproduced by BOT with Fokker–Plank model shows a qualitative agreement with experimental observation. The interplay of diffusion and drag effect is essential to strengthen the clump movement, leading to fast ion distribution function clump-clump interactions. As the value of v_d and v_f are much higher than discharge A, we confirm that main-downward chirping regimes need stronger collision operators. This is consistent with the results in [35] that higher heat ratio could enhance the down-chirping behavior.

The main-downward chirping also shows that clump movement, which indicates energy transfer from wave to particle, is dominant. In many magnetic confinement devices, Alfvén modes were observed with stronger drive, which means main-downward chirping may be excited easier. It explains why main-downward chirping were observed more frequently.

Acknowledgments

This work is supported in part by NNSF of China under Grants No. 11475058, 11405049, 11705049 and 11505053, and by the ITER-CN under Grants No. 2013GB104001 and 2013GB106004.

ORCID iDs

Y.M. Hou https://orcid.org/0000-0001-9086-6841
W. Chen https://orcid.org/0000-0002-9382-6295

References

[1] Fisch N.J. and Herrmann M.C. 1994 *Nucl. Fusion* **34** 1541
[2] Sasaki M. *et al* 2017 *Nucl. Fusion* **57** 036025
[3] Wong K.L. *et al* 1991 *Phys. Rev. Lett.* **66** 1874–7
[4] Heidbrink W.W. *et al* 1991 *Nucl. Fusion* **31** 1635–48
[5] Zarzoso D. *et al* 2013 *Phys. Rev. Lett.* **110** 125002
[6] Sasaki M. *et al* 2017 *Sci. Rep.* **7** 16767
[7] Chen L. and Zonca F. 2016 *Rev. Mod. Phys.* **88** 015008
[8] Heidbrink W.W. 2008 *Phys. Plasmas* **15** 055501
[9] Gorelenkov N.N. *et al* 2014 *Nucl. Fusion* **54** 125001
[10] Breizman B.N. and Sharapov S.E. 2011 *Plasma Phys. Control. Fusion* **53** 054001
[11] Heidbrink W.W. 1995 *Plasma Phys. Control. Fusion* **37** 937
[12] Shinohara K. *et al* 2001 *Nucl. Fusion* **41** 603
[13] Pinches S.D. *et al* 2004 *Plasma Phys. Control. Fusion* **46** S47–57
[14] Fredrickson E.D. *et al* 2006 *Nucl. Fusion* **46** S926
[15] Shi P.W. *et al* 2017 *Phys. Plasmas* **24** 042509
[16] Saigusa M. *et al* 1995 *Plasma Phys. Control. Fusion* **37** 295
[17] Heeter R.F. *et al* 2000 *Phys. Rev. Lett.* **85** 3177
[18] Bernabei S. *et al* 2001 *Nucl. Fusion* **41** 513
[19] Snipes J.A. *et al* 2005 *Phys. Plasmas* **12** 056102
[20] Berk H.L. *et al* 1996 *Phys. Rev. Lett.* **76** 1256
[21] Berk H.L. *et al* 1997 *Phys. Lett.* A **234** 213–8
[22] Lilley M.K. *et al* 2009 *Phys. Rev. Lett.* **102** 195003
[23] Lesur M. *et al* 2009 *Phys. Plasmas* **16** 092305
[24] Lesur M. *et al* 2010 *Phys. Plasmas* **17** 122311
[25] Nguyen C. *et al* 2010 *Plasma Phys. Control. Fusion* **52** 124034
[26] Nguyen C. *et al* 2010 *Phys. Rev. Lett.* **105** 205002
[27] Lilley M.K. *et al* 2010 *Phys. Plasmas* **17** 092305
[28] Lilley M.K. and Breizman B.N. 2012 *Nucl. Fusion* **52** 094002
[29] Lilley M.K. and Nyqvist R.M. 2014 *Phys. Rev. Lett.* **112** 155002
[30] Lesur M. and Idomura Y. 2012 *Nucl. Fusion* **52** 094004
[31] Chen W. *et al* 2010 *Phys. Rev. Lett.* **105** 185004
[32] Chen W. *et al* 2011 *Nucl. Fusion* **51** 063010
[33] Chen W. *et al* 2014 *Nucl. Fusion* **54** 104002
[34] Chen W. *et al* 2016 *Nucl. Fusion* **56** 036018
[35] Bierwage A. *et al* 2017 *Nucl. Fusion* **57** 016036
[36] Zhu J. *et al* 2014 *Nucl. Fusion* **54** 123020
[37] Sharapov S.E. *et al* 2013 *Nucl. Fusion* **53** 104022
[38] Aslanyan V. *et al* 2017 *Phys. Plasmas* **24** 122511
[39] Duarte V.N. *et al* 2017 *Phys. Plasmas* **24** 122508